UC Riverside
UC Riverside Previously Published Works

Title

Effect of Aerosol Size on Glass Transition Temperature

Permalink

https://escholarship.org/uc/item/48j0n6kq

Journal

The Journal of Physical Chemistry Letters, 15(29)

ISSN

1948-7185

Authors

Mahant, Sunandan

Snider, Jefferson R

Petters, Sarah S

et al.

Publication Date

2024-07-25

DOI

10.1021/acs.jpclett.4c01415

Copyright Information

Peer reviewed

Letter

Effect of Aerosol Size on Glass Transition Temperature

Sunandan Mahant, Jefferson R. Snider, Sarah S. Petters, and Markus D. Petters*

ACCESS | Metrics & More | Article Recommendations | SI Supporting Information

ABSTRACT: The amorphous phase state of suspended nanoparticles affects their atmospheric lifetimes and environmental impact. Influence of relative humidity and chemical composition on the glass-to-liquid transition is well-known. However, the influence of the particle size on the phase transition remains uncertain. Here we show experimental data that probe the amorphous phase transition of suspended sucrose particles as a function of particle size. The depression in glass-transition temperature follows the Gibbs−Thomson or Keesom-Laplace predicted proportionality of $\Delta T_g \propto D^{-1}$ for particles 100−700 nm in diameter, but the proportionality changes to $\Delta T_g \propto D^{-1/2}$ for smaller sizes. Literature data for glass-transition temperature depression in thin films and nanoconfined compounds show similar and strong deviations from the expected D^{-1} behavior. While the observed proportionalities remain incompletely understood, the results here provide evidence that the deviation from $\Delta T_g \propto D^{-1}$ is not attributable to substrate effects.
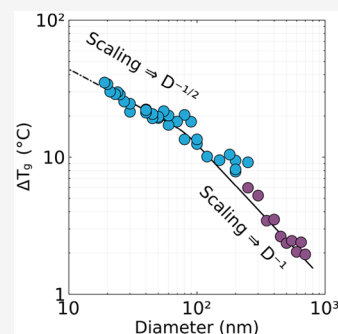
The size dependence of nanoparticle melting point and glass transition is important for many applications including engineered nanomaterials,[1−4] stabilization of pharmaceuticals for drug delivery,[5] the manufacturing of plastics,[6−9] and atmospheric chemistry.[10−12] Phase transition temperature generally decreases as the particle size decreases. Depression in melting point for the first-order phase transition (e.g., crystals melting) is provided by the Gibbs−Thomson equation[13] $\Delta T_m = \frac{6\sigma_{s/l} v_{s,m}}{D \Delta_m S}$, where ΔT_m is the melting temperature depression relative to that of the bulk material, D is the particle diameter, $\sigma_{s/l}$ is the liquid/solid interfacial tension, $v_{s,m}$ is the molar volume of the solid, and $\Delta_m S$ is the molar entropy of the phase change at the melting temperature. Petters and Kasparoglu[10] subsumed the various physicochemical properties into a single parameter:

$$\Delta T_m = \xi_1 D^{-1} \tag{1}$$

where $\xi_1 = \frac{6\sigma_{s/l} v_{s,m}}{\Delta_m S}$ is the Gibbs−Thomson slope parameter. Their analysis of literature data demonstrates that this parameter varies between 300 and 1800 K nm for a wide range of materials.

Gibbs−Thomson is strictly valid only for first-order phase transitions. For second-order transitions, e.g., the glass transition,[14,15] the application of Gibbs−Thomson is less clear. Here we propose that the size dependence of the depression of the glass transition temperature can be modeled using the combination of Keesom's equation,[16] describing the sensitivity of the glass transition temperature to pressure, $\frac{\partial T_g}{\partial p} = T_g \nu \frac{\Delta \alpha}{\Delta c_p}$, and the Laplace equation describing the pressure inside a particle due to curvature,[17] $\Delta p_l = \frac{4\sigma_{l/v}}{D}$:

$$\Delta T_g = \left(\frac{\partial T_g}{\partial p}\right) \Delta p_l = T_{g,bulk} \nu \frac{\Delta \alpha}{\Delta c_p} \frac{4\sigma_{l/v}}{D} = \xi_2 D^{-1} \tag{2}$$

where $T_{g,bulk}$ is the bulk glass transition temperature of the bulk material, ΔT_g is the depression of the glass transition temperature relative to $T_{g,bulk}$, ν is the specific volume, $\Delta \alpha$ is the change in expansion coefficient at the transition, Δc_p is the change in specific heat at the transition, and $\sigma_{l/v}$ is the liquid/vapor interfacial tension. From eq 2, the parameter ξ_2 can be estimated via $\xi_2 = \frac{4\nu \Delta \alpha \sigma_{l/v} T_{g,bulk}}{\Delta c_p}$.

The authors are not aware of any explicit statement of eq 2 in the context of the glass transition temperature depression for nanoparticles in prior studies. One plausible reason is that the predicted inverse-length relationship is not apparent in observational studies of thin-films[18,19] or of materials confined in nanopores.[5,20,21] For example, measurements summarized in Figure 1 show $\Delta T_g \propto h^{-2}$ where h is the film thickness for amorphous polystyrene and polycarbonate. The glass transition temperature depression in amorphous compounds confined in nanopores scales as $\Delta T_g \propto D^{-1/2}$ for nifedipine,[5] $\Delta T_g \propto D^{-1/3}$ for cyanurate,[21] and $\Delta T_g \propto D^{-2/3}$ for polycyanurate, bisphenol-M dicyanate ester, and monocyanate ester (MCE).[20,21] Deviation from $\Delta T_m \propto D^{-1}$ is also reported for lead, tin, and gold nanospheres.[22−24] Various causes could contribute to the phenomenological dependence of ΔT_g on the
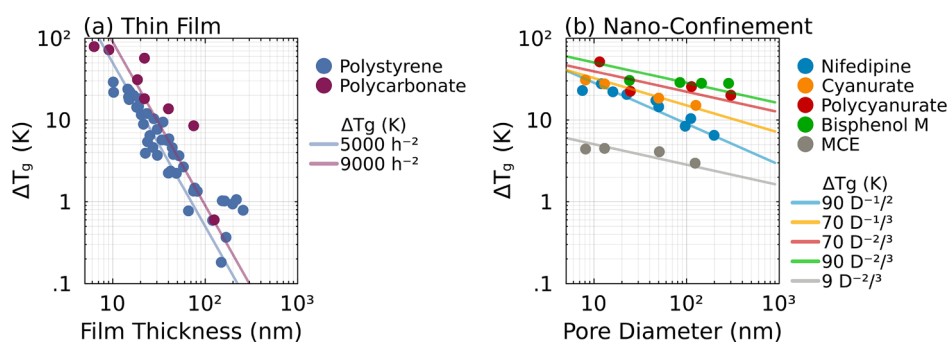
ACS Publications

Figure 1. Depression in T_g with size for (a) thin films[18,19] and (b) compounds confined in nanopores.[5,20,21] Solid lines illustrate the proportionality of ΔT_g with size.
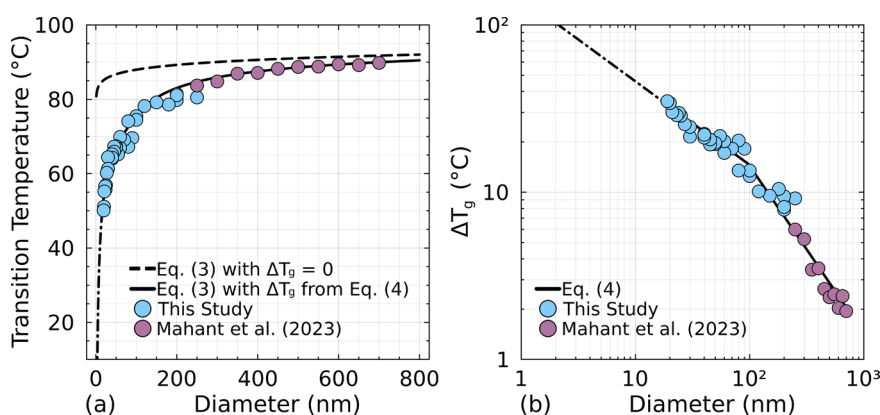

Figure 2. (a) Transition temperature (T_t) and (b) depression in glass transition temperature for sucrose as a function of particle size. Data points from this study are shown in blue while the light purple ones are from Mahant et al. (2023).[41] The dashed line in (a) is eq 3 with $\Delta T_g = 0$. The solid line in (a) is eq 3 with ΔT_g calculated using eq 4. The solid line in (b) is ΔT_g from eq 4. ΔT_g points were calculated by subtracting observed T_t from dashed line in (a). Dash dot line shows extrapolated temperatures for lower diameters.

reciprocal length in nanoparticle studies. These include substrate effects (e.g., difference in interfacial tensions in confined nanopores) or covariability of physicochemical properties with particle size or particle shape.[25] To our knowledge no prior study has reported the influence of particle size on ΔT_g for aerosols with $D < 80$ nm. Importantly, for aerosols substrate effects do not play a role. Studying the phase transition of suspended amorphous nanoparticles may thus provide critical insights into the physical chemistry of this process by removing the potential interactions between the substrate and particle.

Virtanen et al.[26,27] provided the first indirect evidence that amorphous solid organic nanoparticles are common in the atmosphere and that these particles may exist as liquids at diameters less than 17 nm. To better understand this effect, the atmospheric aerosol chemistry community has developed a number of new techniques to study the viscosity in atmospheric samples. The majority of these techniques collect material using filters and apply methods that can measure viscosity on samples of 1 mg or less.[28−33] A handful of techniques have been developed that can measure viscosity for suspended particles.[34−38] These techniques relate the time scale of coalescence to the viscosity and can be performed over a wide range of temperature and relative humidity. There has been indirect evidence that a reduction in particle diameter influences the phase state of atmospheric nanoparticles.[10,12,26] However, to date, no direct measurements have been performed to systematically test how the properties of suspended amorphous nanoparticles depend on particle size

for sizes below 80 nm. This is in part due to the difficulty to conduct controlled size-resolved experiments on aerosol phase state for suspended nanoparticles without working with high number concentrations, which are difficult to generate.[36,38]

This study presents a slightly revised methodology to extend the coalescence approach used by the authors in prior work[35−41] to particles with $D > 20$ nm composed of sucrose. Sucrose is used as a model of viscous organic nanoparticles due to extensive knowledge of its bulk properties, the ease with which it forms amorphous particles, and extensive prior work characterizing the viscosity and fragility of sucrose aerosols.[28,39−42] Here, particle agglomerates are generated by particle generation via atomization[43] or electrospray[44,45] followed by agglomeration via Brownian motion. Agglomerates are classified by electrical mobility to create a stream of nearly monodisperse particles. The sample is heated until particles relaxed into spheres, and this transition is measured using a second mobility analyzer. The corresponding relaxation temperature is termed the transition temperature. At the relaxation time scale of the experiment (11 s), the transition temperature corresponds to a viscosity between 10^6 Pa s and 10^8 Pa s (depending on particle size), which is calculated using Angell scaled fragility and modified Frenkel sintering theory.[35,41,46]

The measured transition temperature T_t depends on the glass transition temperature of the bulk material $T_{g,bulk}$, the viscosity of the material at temperature T_t, the fragility of the material (i.e., the temperature dependence of viscosity), and the depression of glass transition temperature ($\Delta T_g = T_{g,bulk} -$

T_g) at particle diameter D. The relationship between these quantities is derived in the methods section and given by

$$T_t = \frac{T_{g,bulk}}{\left[\frac{(\eta_t + 5)(D_A + 39.17)}{39.17(\eta_t + 5) + 17D_A}\right] - \Delta T_g(D)} \tag{3}$$

where η_t is the $\log_{10}$ value of the viscosity at the transition temperature in units of Pa s, $D_A = 4.7$ is the fragility of dry sucrose,[40] and $T_{g,bulk} = 347$ K is assigned and within the range of the glass transition temperature of dry sucrose from a range of literature sources ($T_{g,bulk} = 341 \pm 18$ K).[42,47−57] Sensitivity of our findings to the assignment $T_{g,bulk} = 347$ K is discussed below. An $\approx 10\%$ increase is expected in D_A due to increased internal pressure at lower diameters,[17,58,59] and accounting for this effect would alter the $T_{g,bulk}$ estimation by <0.5%.

Transition temperature depression, based on paired observations of ΔT_g and D obtained in this study (assuming $T_{g,bulk} = 347$ K), can be described by a single algebraic expression of the form

$$\Delta T_g = \alpha \left(\frac{\delta}{D}\right)^{1/2} \left\{0.5\left[1.0 + \left(\frac{\delta}{D}\right)^{-1/\sigma}\right]\right\}^{-\sigma/2} \tag{4}$$

which corresponds to $\Delta T_g = \alpha \delta^{1/2} D^{-1/2}$ for small D and $\Delta T_g = \alpha \delta D^{-1}$ for large D. The parameter δ corresponds to the diameter where the slope changes and σ determines the width of the transition between the two limiting slopes. Furthermore, we propose $\xi_1 \sim \xi_2 \sim \xi$ (as defined via either eq 1 or eq 2) and $\alpha \delta = \xi$. α, δ, and σ can be derived using nonlinear regression with data weighted proportional to particle diameter, which increases the weight for the less sampled larger particles.

Figure 2a shows the measured T_t as a function of the particle diameter. T_t decreased by ~40 °C from 700 to 19 nm. Some of these measurements are from Mahant et al.,[41] who applied a similar methodology but used an optical particle spectrometer instead of electric mobility measurements to detect the phase transition. Due to the sensitivity limits of the optical particle spectrometer, their results were limited to particles with diameters greater than 250 nm. The dashed line shows the application of eq 3 assuming that $\Delta T_g = 0$, i.e., the glass transition temperature is independent of particle size. Clearly, the T_t decreases more strongly than expected by the combined modified Frenkel theory and Angell scaled fragility. Incorporating ΔT_g size dependence from eq 4 into eq 3 improves the prediction, as shown by the solid curve.

Figure 2b summarizes the ΔT_g that is needed to force agreement between the measured T_t and modeled T_t using eq 3. ΔT_g for data points was calculated by subtracting measured values from the estimated values shown by the dashed line in Figure 2a with $T_{g,bulk} = 347$ K. The depression in values of $\Delta T_{g,bulk}$ for particles >250 nm range is <5 °C. This depression was not analyzed in Mahant et al.[41] in the context of a potential size dependence since these temperature variations are also within the considerable variability in literature reported $T_{g,bulk} = 341 \pm 18$ K for sucrose from a number of different studies.[42,47−57] These authors further assumed that $\Delta T_g = 0$, because the influence of size on melting point is limited to sizes much smaller than 100 nm for crystalline substances.[10] This is wrong. The addition of new measurements reported here demonstrates that the data follow the expected $\Delta T_g \propto D^{-1}$ proportionality for particle sizes of between 700 and 97 nm. At $D < 97$ nm, the scaling changes

from $\Delta T_g \propto D^{-1}$ to $\Delta T_g \propto D^{-1/2}$. Note that the data points for small ΔT_g are sensitive to the assumed $T_{g,bulk}$ value. Reducing the assumed $T_{g,bulk}$ reduces the retrieved ΔT_g for the largest size. For example, changing to $T_{g,bulk} = 345$ K (from the assumed value of 347 K) would correspond to $\Delta T_g = 0$ for the largest diameter measured at 700 nm. This change would not alter the conclusion that $\Delta T_g \propto D^{-1}$ for large particles, $\Delta T_g \propto D^{-1/2}$ for small particles, and that the scale break is at $\delta = 97$ nm.

The data in Figure 2b can be described by using $\alpha = 14.7$ K, $\delta = 97$ nm, and $\sigma = 0.003$. The derived Gibbs−Thomson slope parameter is $\xi \sim 1400$ K nm and well within the range of $300 < \xi < 1800$ K nm reported for the range of compounds summarized in ref 10. The Gibbs−Thomson parameter ξ can, in principle, be calculated either via eq 1 or (2). In practice, this approach is limited by the availability of reliable values for all of the parameters. Specifically, the solid−liquid or liquid−vapor tensions are poorly constrained or unknown under the conditions of the phase transition. Using eq 1, which is strictly applicable for the first-order phase transition, and values of $v_{s/m} = 0.68$ cm^3 g^{-1},[51] $\Delta_m S = \Delta_m H/T_m = \frac{46200}{459}$ J mol^{-1}K^{-1}[60,61] $= 101$ J mol^{-1}K^{-1}, $\sigma_{l/s} = 0.084$ J m^2 (the average value of solid sucrose in liquid melt)[62] gives $\xi_1 = 1165$ K nm, which is close to the observed 1400 K nm for larger particle diameters (>97 nm).

Using eq 2, and the following values for sucrose at the phase transition, $T_{g,bulk} = 347$ K (this study), $v = 6.8 \times 10^{-4}$ m^3 kg^{-1},[51] $\Delta c_p = 755$ J kg^{-1} K^{-1},[63] and $\Delta \alpha = 2.66 \times 10^{-4}$ K^{-1},[16] implies a very high surface tension $\sigma_{l/v} = 4.2$ J m^{-2} to achieve closure with the observed $\xi = 1400$ K nm. Note that this is a different tension from the value given in the methods, which applies to the tension of solid sucrose in a liquid sucrose melt. Such high liquid/vapor (or glass/vapor) tension exceeds values of liquid metals near their melting point.[64] One additional thermodynamic constraint is that not one of the three interfacial tensions (liquid/vapor, solid/vapor, and liquid/solid) can exceed the sum of the other two. Thus, the implication is that both liquid/vapor and solid/vapor tensions are high. Whether such high tensions or the implied internal droplet pressures are realistic is a subject to debate. If true, would imply Laplace pressures inside the droplets that are 50 times larger than those of similarly sized liquid water drops and could have important implications for the behavior of saccharides such as levoglucosan in atmospheric nanoparticles.[17] For example, although condensed-phase direct photolysis is generally suppressed by pressure, radical propagation (within the particle) initiated by surface uptake of gaseous OH radicals is generally accelerated under pressure. Reaction acceleration is balanced by concomitant phlegmatism due to increasing viscosity.[17]

The change in scaling from $\Delta T_g \propto D^{-1}$ to $\Delta T_g \propto D^{-1/2}$ implies that the theory in eqs 1 and (2) is incomplete. The parameter ξ, and thus one or more of the parameters comprising it, appears to be a function of diameter. For the system here, the scale break occurs at $\delta = 97$ nm. This is at a size that is too large to implicate size dependence of physicochemical properties (e.g., surface tension, density, or thermal expansion coefficient), which generally is only important for particles with $D < 15$ nm.[65−69] Nevertheless, the scaling of $\Delta T_g \propto D^{-1/2}$ for small particles is the same as for nifedipine confined in nanopores and the general trend power law dependence with exponents > −1 for all nanopore studies
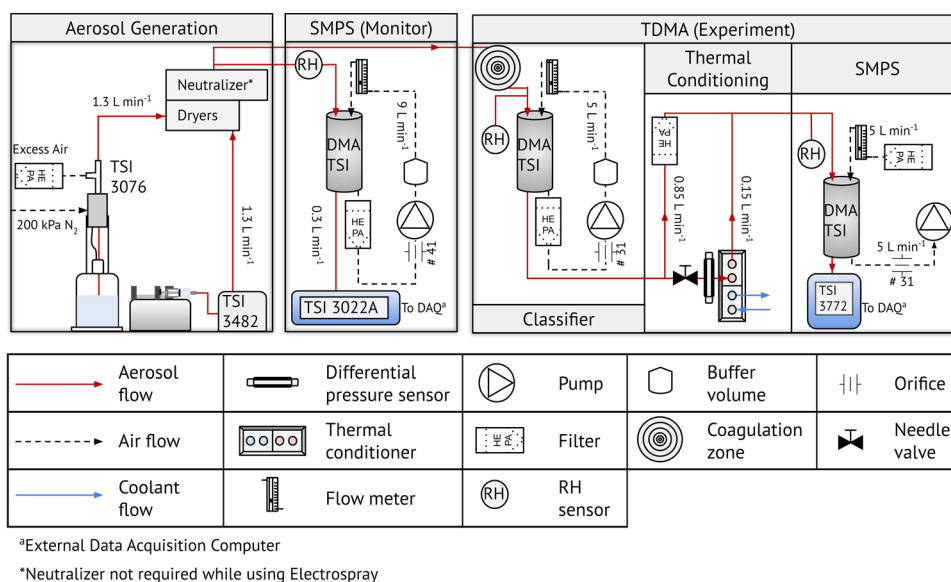
Figure 3. Schematic of experimental setup. Particles through an aerosol generator were monitored by SMPS, passed through a coagulation zone, classified by a DMA, and measured by SMPS after passing through a thermal conditioner.

(Figure 1b). It is unclear whether the $\Delta T_g \propto D^{-1/2}$ scaling holds for sizes $D < 20$ nm. The extrapolation in Figure 2 to smaller sizes remains speculative. The current experimental technique becomes progressively more difficult to apply to smaller sizes due to diminishing shifts in electrical mobility with agglomerate restructuring with size and due to increasing difficulty to create narrow particle size distributions at high enough concentrations to prepare agglomerates. New techniques will be needed to measure viscous phase transition in suspended nanoparticles down to 3 nm in size.

In conclusion, our measurements indicate that, as temperature falls toward a material's glass transition point, the suppression of material stiffening of nanoparticles, which has been shown to follow the inverse diameter proportionality proposed by Gibbs−Thomson (eq 1), follows a shallower decline below the scale break diameter at ∼97 nm (Figure 2b). Results of our experiments corroborate the inverse diameter dependence but also indicate a $D^{-1/2}$ dependence below $D \sim$ 97 nm. However, these data also show that for particles <97 nm, the nanoscale length effects on ΔT_g are generally less strong than the simple $\Delta T_g \propto D^{-1}$ scaling dependence from the Gibbs−Thomson would suggest. The weaker dependence than $\Delta T_g \propto D^{-1}$ is consistent with most available data from the studies summarized in Figure 1, except for the thin-film polymer results. While the observational evidence is not yet fully conclusive, these trends call into question the claim that "atmospheric secondary organic aerosol particles at room temperature are expected to be always liquid at diameters below ∼20 nm",[12] which was made based on an expected D^{-1} proportionality. Currently, the reasons for the deviation from Gibbs−Thomson remain unclear. More empirical studies characterizing ξ and δ for a range of glass-forming compounds are needed in conjunction with efforts to predict ΔT_g from first principles.

■ EXPERIMENTAL METHODS

The experimental methods build on a set of similar experiments performed by the authors.[35,36,39−41,70,71] A schematic of the experimental setup is shown in Figure 3.

Particles were generated using an electrospray (TSI 3482) or an atomizer (TSI 3076) depending on the desired dry diameter (D). The mode diameter was adjusted by changing the solution concentration. For atomized particles, sucrose solutions (0.01% to 0.03% w/w) were prepared in HPLC-grade ultrapure water. For particles generated using electrospray, solutions were prepared as follows: dry sucrose was weighed and dissolved in a 20 mM ammonium acetate buffer (prepared by dissolving ammonium acetate in ultrapure water and adding ammonium hydroxide) solution. Resulting weight fractions ranged from 0.047% to 0.158% w/w where solution strength controlled the mode diameter of generated aerosol size distribution. Particles were dried to relative humidity <20% using silica gel driers and charge neutralized using a bipolar diffusion charger using either ^{210}Po (atomized particles) or soft X-ray (electrospray) as the ion source. Particles are expected to remain in glassy phase at the experimental RH.[33] A Scanning Mobility Particle Sizer (SMPS) was used to monitor the stability of the particle number concentration and size distribution over time. The size distribution was passed through a copper coil ($V = 3$ L, residence time = 180 s) to facilitate particle agglomeration. After passage through the coil, particles were classified by electrical mobility using a Differential Mobility Analyzer (DMA; TSI 3081) operated at a constant voltage. The size was selected from the right tail (larger size) of the generated size distribution, corresponding to the region where particles (agglomerates) formed by Brownian coagulation during passage through the coil. The particle stream was then split between a bypass flow where particles were filtered and a sample flow through a thermal conditioner described in detail in ref 41. The flow through the conditioner ($V = 0.028$ L) was 0.15 L min^{-1} and corresponds to a residence time of 11 s. Thermal conditioner temperature was set before the start of the experiments and ramped at 2 K/min during the experiment until a set end point was reached followed by temperature drop down to the initial set temperature at the same rate. The particle stream was passed through a second SMPS, and its size distribution was monitored during the temperature ramp. The change in D associated with thermal conditioning and

relaxation to spherical shape is the basis for determining the transition temperature.

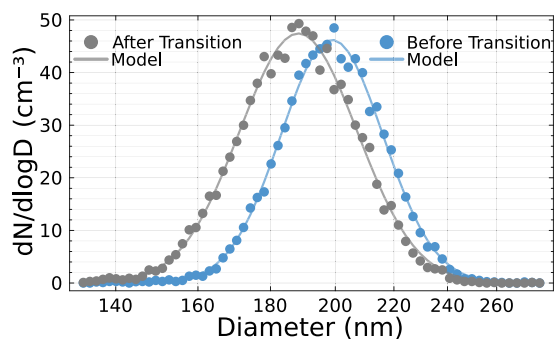Figure 4 shows an example of the observed change in the mobility diameter measured in the second SMPS for the

Figure 4. Measured size distribution before (blue) and after (gray) phase change for a selected mobility diameter of 200 nm. Solid lines correspond to a log-normal fit to the data.

agglomerated particles (blue) and spherical relaxed particles (gray). A log-normal distribution function[72] was fitted to the data to identify the mode diameter. Figure 5 summarizes a single experiment determining T_t. The temperature is linearly ramped from 50 to 100 °C and back to 50 °C over a period of 100 min. The mode diameter extracted from the log-normal fit decreased by ~5% (~10 nm) during the experiment as temperature increased from 75 to 85 °C inside the thermal conditioner. The change is symmetric for the up scan and down scan. The transition temperature is defined as the midpoint of a fit of the mode diameter and conditioner temperature. The fitting function is the form seen in eq 2 in ref 41.

The viscosity at the transition T_t is calculated for each particle size using eq 3 in ref 41 and a residence time in the thermal conditioner $t = 11$ s, interfacial tension of sucrose of 0.084 J m^{-2}, and a shape parameter of 2.5. Viscosity as a function of temperature is calculated using Angell scaled fragility:[40]

$$\log_{10}(\eta) = -5 + 0.434\left(\frac{39.17 D_A}{D_A T/T_g + 39.17 T/T_g - 39.17}\right)$$

(5)

where η (Pa s) is the viscosity, D_A is the fragility parameter, T is the temperature, and T_g is the glass transition temperature.

The viscosity at T_g is 10^{12} Pa s. Taking $\eta_t = \log_{10}$ of the viscosity at temperature T_t setting $T_g = T_{g,bulk} - \Delta T_g(D)$, and solving for T_t yields eq 3.

■ ASSOCIATED CONTENT

■ AUTHOR INFORMATION

Corresponding Author

Markus D. Petters − *Department of Chemical and Environmental Engineering, University of California Riverside, Riverside, California 92521, United States; Center for Environmental Research and Technology (CE-CERT), University of California Riverside, Riverside, California 92507, United States;* ⓞ orcid.org/0000-0002-4082-1693; Email: markus.petters@ucr.edu

Authors

Sunandan Mahant − *Department of Chemical and Environmental Engineering, University of California Riverside, Riverside, California 92521, United States; Center for Environmental Research and Technology (CE-CERT), University of California Riverside, Riverside, California 92507, United States;* ⓞ orcid.org/0000-0002-7953-8094

Jefferson R. Snider − *Department of Atmospheric Sciences, University of Wyoming, Laramie, Wyoming 82072, United States*

Sarah S. Petters − *Department of Chemical and Environmental Engineering, University of California Riverside, Riverside, California 92521, United States; Center for Environmental Research and Technology (CE-CERT), University of California Riverside, Riverside, California 92507, United States;* ⓞ orcid.org/0000-0002-4501-7127

Complete contact information is available at:
https://pubs.acs.org/10.1021/acs.jpclett.4c01415

Author Contributions

The manuscript was written through contributions of all authors. All authors have given approval to the final version of the manuscript.
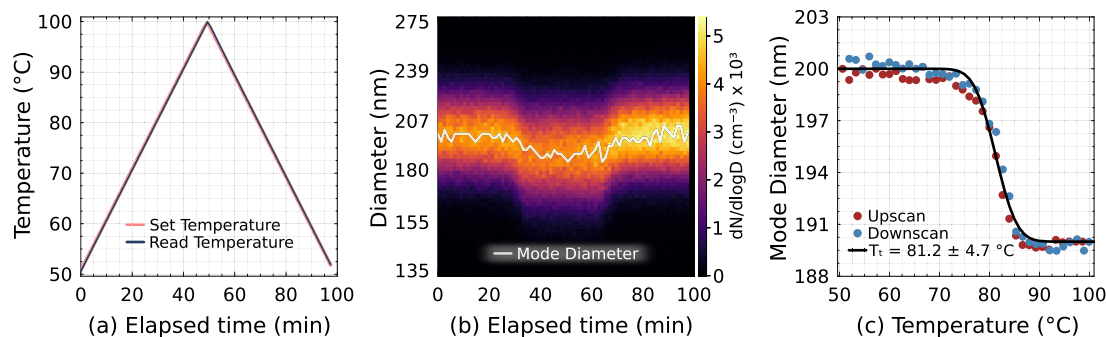

Figure 5. Time series of aerosol size distribution during a 100 min experiment. (a) Temperature profile for the set and read temperature during the experiment. (b) Evolution of the size distribution and mode diameter vs elapsed time. (c) Evolution of the mode diameter derived from the log-normal fit as a function of temperature.

■ REFERENCES

(1) Sheng, H.; Xiao, B.; Jiang, X. Size Dependence of the Phase Transition Temperature of Metal Nanocrystals. *Phys. B Condens. Matter* **2023**, *667*, 415193.

(2) Yu, T.; Shen, Z. X.; Toh, W. S.; Xue, J. M.; Wang, J. Size Effect on the Ferroelectric Phase Transition in SrBi2Ta2O9 Nanoparticles. *J. Appl. Phys.* **2003**, *94* (1), 618−620.

(3) Zhang, W.; Xue, Y.; Fu, Q.; Cui, Z.; Wang, S. Size Dependence of Phase Transition Thermodynamics of Nanoparticles: A Theoretical and Experimental Study. *Powder Technol.* **2017**, *308*, 258−265.

(4) Pal, M.; García Serrano, J.; Santiago, P.; Pal, U. Size-Controlled Synthesis of Spherical TiO$_2$ Nanoparticles: Morphology, Crystallization, and Phase Transition. *J. Phys. Chem. C* **2007**, *111* (1), 96−102.

(5) Cheng, S.; McKenna, G. B. Nanoconfinement Effects on the Glass Transition and Crystallization Behaviors of Nifedipine. *Mol. Pharmaceutics* **2019**, *16* (2), 856−866.

(6) Keddie, J. L.; Jones, R. A. L.; Cory, R. A. Size-Dependent Depression of the Glass Transition Temperature in Polymer Films. *Europhys. Lett. EPL* **1994**, *27* (1), 59−64.

(7) Jiang, Q.; Shi, H. X.; Li, J. C. Finite Size Effect on Glass Transition Temperatures. *Thin Solid Films* **1999**, *354* (1), 283−286.

(8) de Gennes, P. G. Glass Transitions in Thin Polymer Films. *Eur. Phys. J. E* **2000**, *2* (3), 201−205.

(9) Wunderlich, B.; Czornyj, G. A Study of Equilibrium Melting of Polyethylene. *Macromolecules* **1977**, *10* (5), 906−913.

(10) Petters, M.; Kasparoglu, S. Predicting the Influence of Particle Size on the Glass Transition Temperature and Viscosity of Secondary Organic Material. *Sci. Rep.* **2020**, *10* (1), 15170.

(11) Larsen, R. J.; Zukoski, C. F. Effect of Particle Size on the Glass Transition. *Phys. Rev. E* **2011**, *83* (5), 051504.

(12) Cheng, Y.; Su, H.; Koop, T.; Mikhailov, E.; Pöschl, U. Size Dependence of Phase Transitions in Aerosol Nanoparticles. *Nat. Commun.* **2015**, *6*, 5923.

(13) Kaptay, G. The Gibbs Equation versus the Kelvin and the Gibbs-Thomson Equations to Describe Nucleation and Equilibrium of Nano-Materials. *J. Nanosci. Nanotechnol.* **2012**, *12* (3), 2625−2633.

(14) Gibbs, J. H.; DiMarzio, E. A. Nature of the Glass Transition and the Glassy State. *J. Chem. Phys.* **1958**, *28* (3), 373−383.

(15) Wu, J. The Glassy State, Ideal Glass Transition, and Second-Order Phase Transition. *J. Appl. Polym. Sci.* **1999**, *71* (1), 143−150.

(16) Kauzmann, W. The Nature of the Glassy State and the Behavior of Liquids at Low Temperatures. *Chem. Rev.* **1948**, *43* (2), 219−256.

(17) Petters, S. S. Constraints on the Role of Laplace Pressure in Multiphase Reactions and Viscosity of Organic Aerosols. *Geophys. Res. Lett.* **2022**, *49* (12), No. e2022GL098959.

(18) Kim, J. H.; Jang, J.; Zin, W.-C. Thickness Dependence of the Glass Transition Temperature in Thin Polymer Films. *Langmuir* **2001**, *17* (9), 2703−2710.

(19) Shamim, N.; Koh, Y. P.; Simon, S. L.; McKenna, G. B. Glass Transition Temperature of Thin Polycarbonate Films Measured by Flash Differential Scanning Calorimetry. *J. Polym. Sci., Part B: Polym. Phys.* **2014**, *52* (22), 1462−1468.

(20) Li, Q.; Simon, S. L. Surface Chemistry Effects on the Reactivity and Properties of Nanoconfined Bisphenol M Dicyanate Ester in Controlled Pore Glass. *Macromolecules* **2009**, *42* (10), 3573−3579.

(21) Koh, Y. P.; Li, Q.; Simon, S. L. Tg and Reactivity at the Nanoscale. *Thermochim. Acta* **2009**, *492* (1), 45−50.

(22) Wronski, C. R. M. The Size Dependence of the Melting Point of Small Particles of Tin. *Br. J. Appl. Phys.* **1967**, *18* (12), 1731.

(23) David, T. B.; Lereah, Y.; Deutscher, G.; Kofman, R.; Cheyssac, P. Solid-Liquid Transition in Ultra-Fine Lead Particles. *Philos. Mag. A* **1995**, *71* (5), 1135−1143.

(24) Castro, T.; Reifenberger, R.; Choi, E.; Andres, R. P. Size-Dependent Melting Temperature of Individual Nanometer-Sized Metallic Clusters. *Phys. Rev. B* **1990**, *42* (13), 8548−8556.

(25) Letellier, P.; Mayaffre, A.; Turmine, M. Melting Point Depression of Nanosolids: Nonextensive Thermodynamics Approach. *Phys. Rev. B* **2007**, *76* (4), 045428.

(26) Virtanen, A.; Joutsensaari, J.; Koop, T.; Kannosto, J.; Yli-Pirilä, P.; Leskinen, J.; Mäkelä, J. M.; Holopainen, J. K.; Pöschl, U.; Kulmala, M.; Worsnop, D. R.; Laaksonen, A. An Amorphous Solid State of Biogenic Secondary Organic Aerosol Particles. *Nature* **2010**, *467*, 824.

(27) Virtanen, A.; Kannosto, J.; Kuuluvainen, H.; Arffman, A.; Joutsensaari, J.; Saukko, E.; Hao, L.; Yli-Pirilä, P.; Tiitta, P.; Holopainen, J. K.; Keskinen, J.; Worsnop, D. R.; Smith, J. N.; Laaksonen, A. Bounce Behavior of Freshly Nucleated Biogenic Secondary Organic Aerosol Particles. *Atmospheric Chem. Phys.* **2011**, *11* (16), 8759−8766.

(28) Power, R. M.; Simpson, S. H.; Reid, J. P.; Hudson, A. J. The Transition from Liquid to Solid-like Behaviour in Ultrahigh Viscosity Aerosol Particles. *Chem. Sci.* **2013**, *4* (6), 2597−2604.

(29) Hosny, N. A.; Fitzgerald, C.; Vysniauskas, A.; Athanasiadis, A.; Berkemeier, T.; Uygur, N.; Poschl, U.; Shiraiwa, M.; Kalberer, M.; Pope, F. D.; Kuimova, M. K. Direct Imaging of Changes in Aerosol Particle Viscosity upon Hydration and Chemical Aging. *Chem. Sci.* **2016**, *7* (2), 1357−1367.

(30) Kuimova, M. K. Mapping Viscosity in Cells Using Molecular Rotors. *Phys. Chem. Chem. Phys.* **2012**, *14* (37), 12671−12686.

(31) Renbaum-Wolff, L.; Grayson, J. W.; Bertram, A. K. Technical Note: New Methodology for Measuring Viscosities in Small Volumes Characteristic of Environmental Chamber Particle Samples. *Atmospheric Chem. Phys.* **2013**, *13* (2), 791−802.

(32) Kiland, K. J.; Marroquin, K. L.; Smith, N. R.; Xu, S.; Nizkorodov, S. A.; Bertram, A. K. A New Hot-Stage Microscopy Technique for Measuring Temperature-Dependent Viscosities of Aerosol Particles and Its Application to Farnesene Secondary Organic Aerosol. *Atmospheric Meas. Technol.* **2022**, *15* (19), 5545−5561.

(33) Power, R. M.; Reid, J. P. Probing the Micro-Rheological Properties of Aerosol Particles Using Optical Tweezers. *Rep. Prog. Phys.* **2014**, *77* (7), 074601.

(34) Zhang, Y.; Sanchez, M. S.; Douet, C.; Wang, Y.; Bateman, A. P.; Gong, Z.; Kuwata, M.; Renbaum-Wolff, L.; Sato, B. B.; Liu, P. F.; Bertram, A. K.; Geiger, F. M.; Martin, S. T. Changing Shapes and Implied Viscosities of Suspended Submicron Particles. *Atmospheric Chem. Phys.* **2015**, *15* (14), 7819−7829.

(35) Rothfuss, N. E.; Petters, M. D. Coalescence-Based Assessment of Aerosol Phase State Using Dimers Prepared through a Dual-Differential Mobility Analyzer Technique. *Aerosol Sci. Technol.* **2016**, *50* (12), 1294−1305.

(36) Petters, S. S.; Kreidenweis, S. M.; Grieshop, A. P.; Ziemann, P. J.; Petters, M. D. Temperature- and Humidity-Dependent Phase States of Secondary Organic Aerosols. *Geophys. Res. Lett.* **2019**, *46* (2), 1005−1013.

(37) Kasparoglu, S.; Perkins, R.; Ziemann, P. J.; DeMott, P. J.; Kreidenweis, S. M.; Finewax, Z.; Deming, B. L.; DeVault, M. P.; Petters, M. D. Experimental Determination of the Relationship Between Organic Aerosol Viscosity and Ice Nucleation at Upper Free Tropospheric Conditions. *J. Geophys. Res. Atmospheres* **2022**, *127* (16), No. e2021JD036296.

(38) Rothfuss, N. E.; Petters, S. S.; Champion, W. M.; Grieshop, A. P.; Petters, M. D. Characterization of a Dimer Preparation Method for Nanoscale Organic Aerosol. *Aerosol Sci. Technol.* **2019**, *53* (9), 998−1011.

(39) Rothfuss, N. E.; Petters, M. D. Characterization of the Temperature and Humidity-Dependent Phase Diagram of Amorphous Nanoscale Organic Aerosols. *Phys. Chem. Chem. Phys.* **2017**, *19* (9), 6532−6545.

(40) Kasparoglu, S.; Li, Y.; Shiraiwa, M.; Petters, M. D. Toward Closure between Predicted and Observed Particle Viscosity over a Wide Range of Temperatures and Relative Humidity. *Atmospheric Chem. Phys.* **2021**, *21* (2), 1127−1141.

(41) Mahant, S.; Iversen, E. M.; Kasparoglu, S.; Bilde, M.; Petters, M. D. Direct Measurement of the Viscosity of Ternary Aerosol Mixtures. *Env. Sci. Atmos* **2023**, *3* (3), 595−607.

(42) Rothfuss, N. E.; Petters, M. D. Influence of Functional Groups on the Viscosity of Organic Aerosol. *Environ. Sci. Technol.* **2017**, *51* (1), 271−279.

(43) Liu, B. Y. H.; Lee, K. W. An Aerosol Generator of High Stability. *Am. Ind. Hyg. Assoc. J.* **1975**, *36* (12), 861−865.

(44) Rulison, A. J.; Flagan, R. C. Electrospray Atomization of Electrolytic Solutions. *J. Colloid Interface Sci.* **1994**, *167* (1), 135−145.

(45) Chen, D.-R.; Pui, D. Y. H.; Kaufman, S. L. Electrospraying of Conducting Liquids for Monodisperse Aerosol Generation in the 4 Nm to 1.8 Mm Diameter Range. *J. Aerosol Sci.* **1995**, *26* (6), 963−977.

(46) Pokluda, O.; Bellehumeur, C. T.; Vlachopoulos, J. Modification of Frenkel's Model for Sintering. *AIChE J.* **1997**, *43* (12), 3253−3256.

(47) Tiers, G. V. D. Materials Science of Organic Compounds: Part 3. Glass-Formers, Vitriphores, Tg, and Molecular Chirality. *Thermochim. Acta* **1993**, *226*, 317−324.

(48) Buitink, J.; van den Dries, I. J.; Hoekstra, F. A.; Alberda, M.; Hemminga, M. A. High Critical Temperature above *Tg* May Contribute to the Stability of Biological Systems. *Biophys. J.* **2000**, *79* (2), 1119−1128.

(49) Elamin, A. A.; Sebhatu, T.; Ahlneck, C. The Use of Amorphous Model Substances to Study Mechanically Activated Materials in the Solid State. *Int. J. Pharm.* **1995**, *119* (1), 25−36.

(50) Saleki-Gerhardt, A.; Zografi, G. Non-Isothermal and Isothermal Crystallization of Sucrose from the Amorphous State. *Pharm. Res.* **1994**, *11* (8), 1166−1173.

(51) Simperler, A.; Kornherr, A.; Chopra, R.; Bonnet, P. A.; Jones, W.; Motherwell, W. D. S.; Zifferer, G. Glass Transition Temperature of Glucose, Sucrose, and Trehalose: An Experimental and in Silico Study. *J. Phys. Chem. B* **2006**, *110* (39), 19678−19684.

(52) Kawai, K.; Hagiwara, T.; Takai, R.; Suzuki, T. Comparative Investigation by Two Analytical Approaches of Enthalpy Relaxation for Glassy Glucose, Sucrose, Maltose, and Trehalose. *Pharm. Res.* **2005**, *22* (3), 490−495.

(53) Miller, D. P.; de Pablo, J. J. Calorimetric Solution Properties of Simple Saccharides and Their Significance for the Stabilization of Biological Structure and Function. *J. Phys. Chem. B* **2000**, *104* (37), 8876−8883.

(54) Shamblin, S. L.; Tang, X.; Chang, L.; Hancock, B. C.; Pikal, M. J. Characterization of the Time Scales of Molecular Motion in Pharmaceutically Important Glasses. *J. Phys. Chem. B* **1999**, *103* (20), 4113−4121.

(55) Orford, P. D.; Parker, R.; Ring, S. G. Aspects of the Glass Transition Behaviour of Mixtures of Carbohydrates of Low Molecular Weight. *Carbohydr. Res.* **1990**, *196*, 11−18.

(56) Roos, Y. Melting and Glass Transitions of Low Molecular Weight Carbohydrates. *Carbohydr. Res.* **1993**, *238*, 39−48.

(57) Murthy, S. S. N.; Gangasharan; Nayak, S. K. Novel Differential Scanning Calorimetric Studies of Supercooled Organic Liquids. *J. Chem. Soc. Faraday Trans.* **1993**, *89* (3), 509−514.

(58) Pawlus, S.; Paluch, M.; Ziolo, J.; Roland, C. M. On the Pressure Dependence of the Fragility of Glycerol. *J. Phys.: Condens. Matter* **2009**, *21* (33), 332101.

(59) Kaminski, K.; Pawlus, S.; Adrjanowicz, K.; Wojnarowska, Z.; Wlodarczyk, P.; Paluch, M. The Importance of the Activation Volume for the Description of the Molecular Dynamics of Glass-Forming Liquids. *J. Phys.: Condens. Matter* **2012**, *24* (6), 065105.

(60) Sopade, P. A.; Kearsley, M. W.; LeGrys, G. A. Heat of Melting Sucrose. *Int. Sugar J.*, **1988**, *90*

(61) *CRC Handbook of Chemistry and Physics: A Ready-Reference Book of Chemical and Physical Data*, 79th ed.; Lide, D. R., Ed.; CRC: Boca Raton, FL, 1998.

(62) Hook, A. V.; Kilmartin, E. J. The Surface Energy of Sucrose. *Z. Für Elektrochem. Berichte Bunsenges. Für Phys. Chem.* **1952**, *56* (4), 302−305.

(63) Magoń, A.; Wurm, A.; Schick, C.; Pangloli, Ph.; Zivanovic, S.; Skotnicki, M.; Pyda, M. Heat Capacity and Transition Behavior of Sucrose by Standard, Fast Scanning and Temperature-Modulated Calorimetry. *Thermochim. Acta* **2014**, *589*, 183−196.

(64) Volpp, J. Surface Tension of Steel at High Temperatures. *SN Appl. Sci.* **2023**, *5* (9), 237.

(65) Tolman, R. C. The Effect of Droplet Size on Surface Tension. *J. Chem. Phys.* **1949**, *17* (3), 333−337.

(66) Lu, H. M.; Jiang, Q. Size-Dependent Surface Tension and Tolman's Length of Droplets. *Langmuir* **2005**, *21* (2), 779−781.

(67) Xu, S.; Scherer, G. W.; Mahadevan, T. S.; Garofalini, S. H. Thermal Expansion of Confined Water. *Langmuir* **2009**, *25* (9), 5076−5083.

(68) Dobrzanski, C. D.; Gurevich, B.; Gor, G. Y. Elastic Properties of Confined Fluids from Molecular Modeling to Ultrasonic Experiments on Porous Solids. *Appl. Phys. Rev.* **2021**, *8* (2), 021317.

(69) Flores Roman, S. A.; Barbosa, G. D.; Gor, G. Y. Elasticity of Confined Simple Fluids from an Extended Peng-Robinson Equation of State. *Ind. Eng. Chem. Res.* **2023**, *62* (22), 8972−8980.

(70) Marsh, A.; Petters, S. S.; Rothfuss, N. E.; Rovelli, G.; Song, Y. C.; Reid, J. P.; Petters, M. D. Amorphous Phase State Diagrams and Viscosity of Ternary Aqueous Organic/Organic and Inorganic/Organic Mixtures. *Phys. Chem. Chem. Phys.* **2018**, *20* (22), 15086−15097.

(71) Kasparoglu, S.; Islam, M. M.; Meskhidze, N.; Petters, M. D. Characterization of a Modified Printed Optical Particle Spectrometer for High-Frequency and High-Precision Laboratory and Field Measurements. *Atmospheric Meas. Technol.* **2022**, *15* (17), 5007−5018.

(72) Seinfeld, J. H.; Pandis, S. N. *Atmospheric Chemistry and Physics: From Air Pollution to Climate Change*, 3rd ed.; Wiley: Hoboken, NJ, 2016.